

Status of the MIPP NuMI Target Data Analysis

Jonathan M. Paley, Ph. D., for the MIPP Collaboration

Argonne National Laboratory, HEP Division, 9700 South Cass Avenue, Argonne, IL, USA

E-mail: jpaley@anl.gov

Abstract. The fixed-target Main Injector Particle Production (MIPP) Experiment was designed to produce large sets of hadron production data on variety of nuclear targets using a range of beam particles and momenta. The spectrometer has excellent momentum resolution, and particle identification is determined for particles ranging between 0.3 - 80 GeV/c using dE/dx , time-of-flight and Cherenkov radiation measurements. MIPP collected $\sim 1.6 \times 10^6$ events of 120 GeV Main Injector protons striking a spare NuMI target. This talk will review the experimental setup, performance of the detectors, and preliminary results of the measurement of pion and Kaon yields from the NuMI target data.

1. Introduction

Hadron production uncertainties in MC simulations generally dominate the uncertainties of NuMI flux predictions at the level of 15-20%, and is a limiting factor in the neutrino cross-section measurements being done by many NuMI-based experiments. Direct measurements of hadron production can be used to improve MC simulations and reduce the uncertainties of the flux predictions. The Main Injector Particle Production (MIPP) Experiment at Fermi National Accelerator Laboratory (FNAL) collected data between December 2004 and February 2006 on a variety of fixed-target nuclei with a tertiary beam consisting of tagged protons, charged pions and charged kaons over a momentum range from 5-120 GeV/c. One of the goals of the experiment was to measure the hadron production yield off of an actual NuMI target with 120 GeV/c (Main Injector) protons, which is the focus of this paper.

2. The MIPP Spectrometer, Event Reconstruction and Particle Identification

The MIPP Experiment uses a full acceptance spectrometer with two analysis magnets for momentum determination, a 1.5 m long TPC located just downstream of the interaction region, and 4 drift chambers and 2 proportional wire chambers located further downstream for particle tracking. The TPC sits inside one of the spectrometer dipole magnets. The spectrometer magnets deflect charged particles in opposite direction. Three wire chambers upstream of the target are used to track incident beam particles. All tracking detectors have $\mathcal{O}(\text{mm})$ resolution in the transverse direction. Trajectories of secondary charged particles are first reconstructed using TPC data in three dimensions. These tracks are then projected downstream and matched to nearby hits in the tracking wire chambers. The final momentum and charge of the particle is determined from the bends of the reconstructed trajectories through the magnets.

In the analysis of the NuMI target data, Monte Carlo simulation studies with a detailed description of the spectrometer geometry indicate that the momentum resolution is $< 5\%$, and the transverse momentum resolution is $< 20 \text{ MeV}/c$ for all momenta. The absolute momentum

scale is determined from distributions of the reconstructed K^0 s invariant mass and of the reconstructed momentum of beam protons (120 GeV/c protons from the Main Injector), which in both cases agree to within 1% of the expected values.

MIPP was designed to provide particle identification with $2 - 3\sigma$ separation across the momentum range of a few hundred MeV to ≥ 80 GeV using $\langle dE/dx \rangle$ information from the TPC (0.2-1.2 GeV/c), a plastic scintillator-based time-of-flight (ToF) detector (0.5-2.5 GeV/c), a segmented gas Cherenkov (Ckov) detector (2-20 GeV/c) and a gas ring imaging Cherenkov (RICH) detector (4-80 GeV/c). The $\langle dE/dx \rangle$ is determined for every reconstructed track, and provides clean separation of π and p between 0.2 and 1.2 GeV/c. The ToF provides $\pi - p$ separation up to about 2 GeV/c. However, due to the high multiplicities of secondaries in the NuMI data set, many particle trajectories pass through the same ToF channels and it is impossible to disentangle the particles in the ToF data. Therefore only a subset of ToF data are usable. Although the Ckov detector is made of 96 mirror which reflect the light produced inside the gas volume onto PMTs, this detector also suffers from the same high multiplicity problem as the ToF; approximately 50% of all particles passing through the detector coming off the NuMI target share light with another particle. Finally, particles in the RICH detector produce light cones which are reflected to form a ring of light on an array of ~ 2300 1/2" PMTs. The high segmentation of the RICH detector allows for multiple rings to be clearly distinguished and matched to reconstructed tracks, therefore the high multiplicities of secondaries is not an issue for this detector. The RICH detector allows for clean pion identification beginning above 4 GeV/c, and clean kaon identification above 20 GeV/c.

3. NuMI Target Analysis

The goal of this analysis is the measurement of the charged pion yield off the surface of the NuMI target. The total number of charged pions is determined as a function of (p_z, p_T) of the particle, and the measurement will cover a broad range of momenta, from $\sim 0.5 - 80$ GeV/c. Currently, the analysis sums over the longitudinal position of the pions as they exit the surface of the target. Also, the particle identification information from the Ckov detector are not used in the analysis. Information from the ToF detector were also not used at the time this paper was presented, although studies are underway to determine ways to make use of the ToF measurements in combination with TPC $\langle dE/dx \rangle$ measurements. This analysis therefore will provide measurements of pion yields using the TPC $\langle dE/dx \rangle$ and RICH ring radius (converted to m^2) measurements from 300 MeV/c to 80 GeV/c, with some gaps in between that would otherwise be covered by the ToF and Ckov detectors.

3.1. (p_z, p_T) Bins, and Reconstruction Efficiency and PID Acceptance Corrections

The binning in (p_z, p_T) is based on the requirement that the statistical uncertainty of the number of pions in a bin is $\sim 5\%$ or less. Furthermore the number of bins at lower momenta, where statistics are not an issue, is limited in order to reduce the amount of computations made in the analysis. So far no physics motivation has been identified to use finer binning at lower momentum. A total of 76 bins are defined in this analysis, covering 300 MeV - 80 GeV/c.

Geometric acceptance and reconstruction efficiency corrections are determined using MC simulations which has detailed descriptions of the target and spectrometer and detector geometries. The combined geometric acceptance of the spectrometer and the reconstruction efficiency are shown in Fig. 1(a) as a function of (p_z, p_T) . Fig. 1(b) shows the geometric acceptance of the PID detectors. In both plots, the numbers in the boxes refers to a bin number (0-75); the color of the boxes indicates the scale on the z-axis of the plots, where 100% efficiency or acceptance is red and violet represents 0. Both plots show results for negative particles; positively charged particles have very similar efficiencies and acceptances. All reconstructed tracks have a measurement of $\langle dE/dx \rangle$ by definition, therefore at low momentum where the

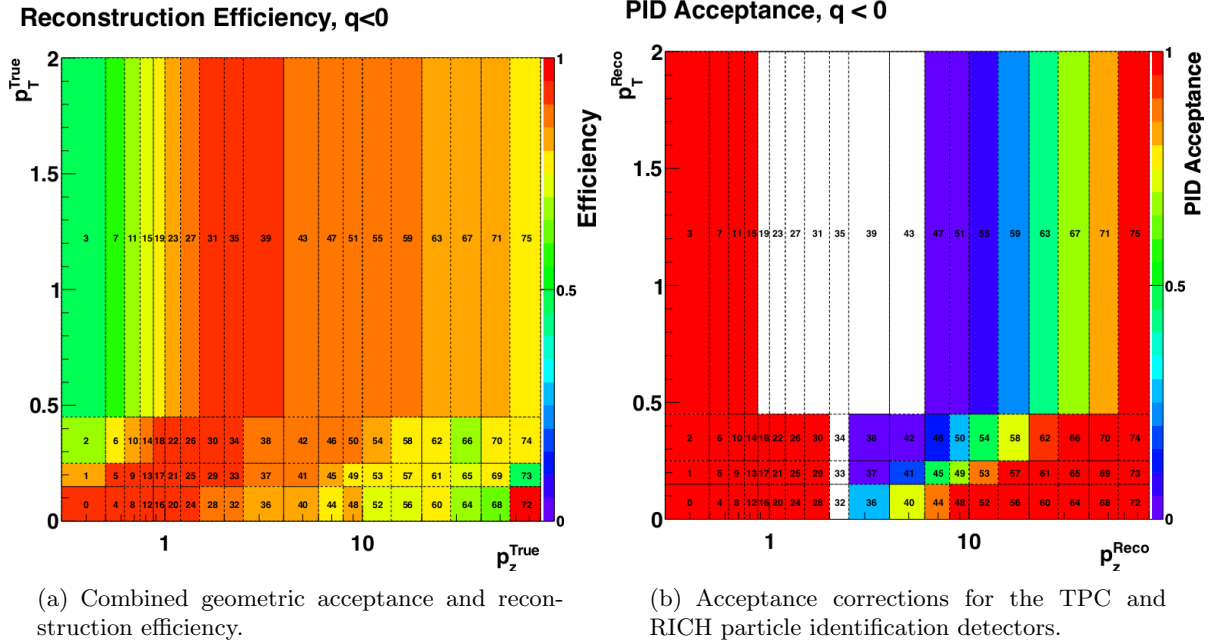


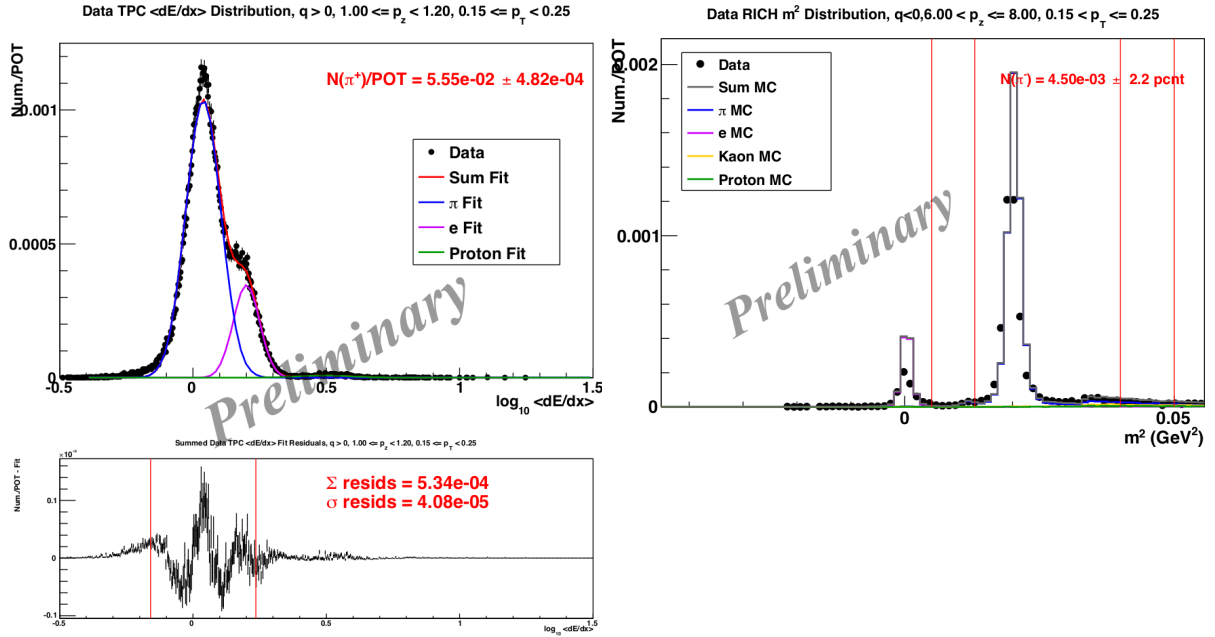
Figure 1. Acceptances and reconstruction efficiencies as a function of (p_z, p_T) as determined from MC simulation. The numbers in the boxes refer to a bin number, the colors represent the efficiency (red=100%, green=50%).

$\langle dE/dx \rangle$ is used for PID, the acceptance is 100%. On the other hand, measurements in the RICH detector require particles to traverse finite-sized windows at the front and back of the detector, and so not all particles satisfy this condition. This is particularly true for lower momentum particles and is the reason for the low acceptance in the RICH PID detector at low momenta. The white bins in Fig. 1(b) indicate those bins for which we do not have a means to identify pions.

3.2. PID Detector Measurements

Fig. 2(a) shows an example of how the pion yield is determined from $\langle dE/dx \rangle$ measurements at low momenta. The distribution of $\log(\langle dE/dx \rangle)$ of a particle type in a (p_z, p_T) bin is well described by a Gaussian function. Therefore, the pion yield is obtained from TPC $\langle dE/dx \rangle$ measurements by fitting the distribution of $\log_{10}(\langle dE/dx \rangle)$ of all particles in each (p_z, p_T) bin to a sum of three Gaussian functions, one each for pions, electrons and protons (the kaon contribution is immeasurable). The pion yield is therefore the integral of the fitted pion Gaussian peak (the one with the lowest average $\langle dE/dx \rangle$). To account for the fact that the distribution is not exactly Gaussian, residuals are calculated for the full 3 Gaussian fit function, and a correction is estimated as the sum across 3σ of the of the pion-only peak. The uncertainty on that correction is estimated as the RMS of the residuals across the same range. As Fig. 2(a) shows, the non-Gaussian corrections and uncertainties are very small compared to the integral of the pion Gaussian peak. At the time this paper was presented, the $\langle dE/dx \rangle$ distributions of positive and negative particles in each (p_z, p_T) bin were fit independently. The distributions of $\langle dE/dx \rangle$ from positive and negative particles in the same (p_z, p_T) bin are now fit simultaneously, which helps constrains the fit for the $\langle dE/dx \rangle$ distribution for \bar{p} 's.

The pion yield at higher momenta is determined using reconstructed RICH ring radii, converted to m^2 distributions. These distributions are not well described by Gaussians, however the pion peak is typically very well separated from all other particles, and so a cut-and-count



(a) $\langle dE/dx \rangle$ distribution for one (p_z, p_T) bin. The distribution is fit to a sum of three Gaussian functions, one each for π, p and e (top). The pions in this bin form the first peak. Residuals (bottom) are used to estimate corrections and uncertainties due to the non-Gaussian features of the distribution.

(b) RICH m^2 distribution for one (p_z, p_T) bin. Data are shown in the black dots, MC is shown in the solid histograms. Both are normalized to protons on target (POT). The pion peak is the larger of the two and is very well separated from the electron peak. MC reweighted by data in two sidebands near the pion peak are used to correct for backgrounds in the signal region.

Figure 2. Particle identification distributions from the TPC (left) and RICH (right) detectors, each for one (p_z, p_T) bin.

approach is taken in this analysis. Fig. 2(b) shows an example of this approach. Windows are defined that encompass the pion signal peak, and two sideband windows are defined that are used to estimate corrections and uncertainties due to backgrounds in the signal window. We assume the shapes of the background and signal is adequately described by the MC simulation, and use the data in the sidebands to renormalize the MC background prediction. A very conservative 30% uncertainty on the ratio of the signal to background in the MC is assumed, which results in typically very small (1-2%) systematic uncertainties in this approach. The cut-and-count approach used here is implemented in a way that the combined statistical and systematic uncertainty of the background subtraction is determined simultaneously.

Using these two approaches to determine the pion yields from TPC and RICH detector measurements, we find that at low momentum the uncertainties are at the 1% level or less, and at higher momentum, most (p_z, p_T) bins have uncertainties that are $\leq 10\%$. There are a few (p_z, p_T) bins where the uncertainties are $\geq 10\%$, driven completely by statistics.

4. Conclusion

We present here a simplified analysis of data collected in the MIPP experiment using an actual NuMI target that will produce pion yields across a broad range of momenta. Nearly all the pieces are in place to finalize the analysis, including the determination of the pion yield, efficiency and acceptance corrections, and some systematic uncertainties. Studies of other systematic uncertainties are underway, and results will be forthcoming.